



Original Paper

The occurrence characteristics of oil in shales matrix from organic geochemical screening data and pore structure properties: An experimental study



Zi-Zhi Lin ^{a, b}, Jun-Qian Li ^{a, b}, Shuang-Fang Lu ^{c, a, b, *}, Qin-Hong Hu ^{a, b},
Peng-Fei Zhang ^{d, **}, Jun-Jie Wang ^{a, b}, Qi Zhi ^{a, b}, Hong-Sheng Huang ^{a, b}, Na Yin ^{a, b},
Yue Wang ^d, Tian-Chen Ge ^d

^a National Key Laboratory of Deep Oil and Gas, China University of Petroleum (East China), Qingdao 266580, Shandong, China

^b School of Geosciences, China University of Petroleum (East China), Qingdao 266580, Shandong, China

^c Sanya Offshore Oil & Gas Research Institute, Northeast Petroleum University, Sanya 572025, Hainan, China

^d College of Earth Science and Engineering, Shandong University of Science and Technology, Qingdao 266590, Shandong, China

ARTICLE INFO

Article history:

Received 14 September 2022

Received in revised form

6 March 2023

Accepted 4 September 2023

Available online 9 September 2023

Edited by Jie Hao and Teng Zhu

Keywords:

Shale oil

Occurrence characteristics

Sequential solvent extraction

Low-temperature nitrogen adsorption

Funing Formation

Dongtai Depression

ABSTRACT

The occurrence characteristics of shale oil are of great significance to the movability of shale oil. In this study, the occurrence characteristics of oil in the shale matrix at Funing Formation shale in Subei Basin were quantitatively evaluated by organic geochemistry and microscopic pore structure characterization experiments. The Multiple Isothermal Stages Pyrolysis (MIS) experiment results show that the content of total oil, adsorbed oil, and free oil in the shales are 3.15–11.25 mg/g, 1.41–4.95 mg/g, and 1.74–6.51 mg/g, respectively, among which the silicon-rich shale has the best oil-bearing. The relative content of free oil shows an increasing trend in pores with pore diameters greater than 3 nm. When the relative content of free oil reaches 100%, the pore size of silicon-rich shale is about 200 nm, while that of calcium-rich shale, clay-rich shale, and siliceous mixed shale is about 10 nm. The occurrence law of adsorbed oil is opposite to that of free oil, which indicates that shale oil will occur in the pores and fractures in a free state in a more extensive pore size range (>200 nm). This study also enables us to further understand the occurrence characteristics of shale oil under the interaction of occurrence state and occurrence space.

© 2023 The Authors. Publishing services by Elsevier B.V. on behalf of KeAi Communications Co. Ltd. This is an open access article under the CC BY-NC-ND license (<http://creativecommons.org/licenses/by-nc-nd/4.0/>).

1. Introduction

Shale oil refers to oil that occurs in organic-rich shale formations with no natural production capacity or lower than the lower limit of industrial oil production and requires special technological measures to obtain industrial oil production (Jia et al., 2012; Chen, 2017; Feng et al., 2020; Hu et al., 2020; Lin et al., 2022; Xu et al., 2022). The occurrence state of shale oil can be classified as the free state, adsorbed state, and a small amount of inter-miscible state (dissolved in natural gas, kerogen, residual water, etc.) (Lu et al., 2016;

Ning et al., 2017; Wang et al., 2019; Zhu et al., 2021). Adsorbed oil mainly refers to oil attached to surfaces of mineral particles or organic matter. Explaining this part of shale oil is almost impossible, and it is considered virtually immovable with current development technology. Free oil mainly occurs in pores and fractures of the mineral matrix. It is the main contributor to shale oil productivity under the natural elastic energy recovery method, which means that the occurrence state of shale oil is an essential factor affecting the mobility of shale oil (Jiang et al., 2016; Li et al., 2017, 2018; Hu et al., 2021a). Moreover, the composition of shale oil is very complex: it generally consists of more than 50% saturated hydrocarbons and also contains a certain content of polar compounds and aromatic hydrocarbons (Regtop et al., 1982; Zhang et al., 2020); therefore, the evaluation of shale oil content (i.e., adsorbed oil and free oil) and proportion in different occurrence states is of great significance for determining the mobility and

* Corresponding author. Sanya Offshore Oil & Gas Research Institute, Northeast Petroleum University, Sanya 572025, Hainan, China.

** Corresponding author.

E-mail addresses: lushuangfang@nepu.edu.cn (S.-F. Lu), zhangpengfei0907@sdust.edu.cn (P.-F. Zhang).

production potential of shale oil (Lu et al., 2016).

At present, Numerous quantitative evaluation methods for shale oil in different occurrence states are widely used, e.g. Standard Rock-Eval (RE) Pyrolysis (Jarvie, 2012; Jiang et al., 2016; Abrams et al., 2017; Wang et al., 2022), Multiple Isothermal Stages (MIS) Pyrolysis (Romero-Sarmiento et al., 2016; Zink et al., 2016), Sequential Solvent Extraction (SSE) (Schwark et al., 1997; Pan and Liu, 2009) and other methods (Li et al., 2018). Rock pyrolysis (RE and MIS) has also been widely used in shale oil resource evaluation to assess in-situ hydrocarbon content rapidly (Hu et al., 2018, 2021b). The principle of the sequential solvent extraction technique is that shale oil with different occurrence states has different occurrence spaces and molecular polarity. Then different polar solvents are used to extract shale oil with different occurrence states in shale to obtain the content of free and adsorbed oil. The SSE technique was first used to characterize the fractionation of bitumen in source rocks. Since then, many scholars have used this method to extract samples of different particle sizes to obtain hydrocarbon fractions with different occurrence states (Sajgó et al., 1983; Wilhelms et al., 1996; Pan and Liu, 2009; Yu et al., 2017). The MIS pyrolysis and SSE methods assume that free shale oil is mainly small molecules, weakly polar hydrocarbons, or non-hydrocarbon compounds occurring in fractures or large pores. In contrast, the adsorbed shale oil is mainly composed of macromolecules, polar hydrocarbons, or non-hydrocarbon compounds in micropores or kerogen. In addition, researchers have also conducted many studies on the occurrence space of shale oil. The mainstream research methods include environmental scanning electron microscopy (ESEM), nitrogen adsorption before and after oil washing (B-AOWNA), two-dimensional nuclear magnetic resonance (2D-NMR), etc. (Liu et al., 2019; Wang et al., 2019; Dang et al., 2022; Zhang et al., 2022a,b). Among them, ESEM is mainly used to qualitatively analyze the occurrence space of shale oil, while B-AOWNA and 2D-NMR technology can quantitatively characterize the occurrence space of shale oil.

Although these methods reveal the occurrence characteristics of shale oil to a certain extent, most of them only perform a single analysis of the content of shale oil in different occurrence states or the occurrence space or pore size distribution (PSD) of shale oil. SSE and rock pyrolysis can only reveal the content of shale oil in different occurrence states, but cannot quantitatively characterize its occurrence space or PSD. There is still a lack of effective research on the occurrence characteristics of rock oil under the coupling effect of different occurrence states and PSD.

This paper intends to evaluate the occurrence characteristics of shale oil by combining geochemical analysis with shale pore structure characterization methods. Standard RE pyrolysis and sequential solvent extraction techniques were performed to comprehensively reveal the content of shale oil in different occurrence states. While quantifying the content of shale oil in different occurrence states, low-temperature nitrogen adsorption technology was also carried out to characterize the occurrence space and PSD of shale oil in different occurrence states. Through the organic geochemical analysis and pore structure characterization technology, the occurrence characteristics of shale oil under the coupled effects of different occurrence states and PSD are clarified. This research allows a more detailed understanding of the occurrence characteristics of shale oil and provides some theoretical guidance for improving the recovery and economic development.

2. Geological setting

The Northern Jiangsu Basin, with an area of 35000 km², is faulted in eastern China (Fig. 1). The Gaoyou Sag is a sub-basin located in the south of the Northern Jiangsu Basin and covers an

area of 2670 km². Gaoyou Sag is bounded by Tianchang Uplift, Lingtangqiao Low Uplift, Liubao Low Uplift on the west, Tongyang Uplift on the South, and Wubao Low Uplift in the East. Jinhu Sag is the most considerable sag in the continental part of the Northern Jiangsu Basin (Fig. 1), which is bounded on the north by Jianhu Uplift, on the south by the Yangcun Fault zone, and Tianchang Uplift, on the west by Zhangbaling Uplift, and on the east by Lintangqiao-Liubao Uplift. (Gang et al., 2012; Dong et al., 2013; Liu et al., 2014; Zhang et al., 2022a,b).

The Funing Formation formed a lacustrine sedimentary system dominated by argillaceous sediments, with a thickness of 200–1500 m. The shale of the second member (E₁f₂) is the primary source rock of the Funing Formation, and its lithology is mainly dark gray or gray-black mudstone mixed with argillaceous limestone, thin limestone, sandstone, or dolomite. The organic matter types of the shale in E₁f₂ are mainly Type I and Type II, and the maturity is greater than 0.8%. The organic carbon content is mainly distributed in 1%–2%, and the mass fraction of chloroform asphalt "A" is between 0.1% and 0.3%. Several wells in the E₁f₂ have obtained industrial oil flow through the oil test, which has favorable conditions for the formation of shale oil (Liu et al., 2014).

3. Samples and methodology

3.1. Samples

In this study, six samples from the E₁f₂ were selected from three cored wells in the Gaoyou Sag and Jinhu Sag. According to the three terminal element diagram of the main minerals (quartz & feldspar, calcite & dolomite, and clays), the lithological division scheme of shale in the E₁f₂ was established in Fig. 2a–f represents clay-rich shale, silicon-rich shale, calcium-rich shale, clayed mixed shale, siliceous mixed shale, and calcareous mixed shale, respectively, and the total organic carbon (TOC) increases from blue to red. Four lithological types were identified in the samples: HX4-3, QX4-1, and QX4-2 are silicon-rich shale, SX84-8 is clay-rich shale, SX84-20 is calcium-rich shale, and SX84-27 is siliceous mixed mudstone.

3.2. Methodology

3.2.1. Field emission scanning electron microscopy (SEM)

SEM analysis yields a visual depiction of pore types and was used for accurate characterization of pore structure. The experiments were performed at FFI Quanta 200 F field emission-scanning electron microscope. Samples were obtained from the same position as the other experiments and the irregular samples with a size of approximately 1 cm³ were mounted on stubs and hand-polished. Subsequently, the samples were polished with an argon-ion beam to produce a flat and smooth surface, and all samples were coated with a layer of Au (99.999% purity) approximately 10 nm thick. A series of back-scattered electron (BSE) and secondary electron (SE) images were obtained at a resolution ranging from 1.04 nm to 558 nm.

3.2.2. Low-temperature nitrogen adsorption

Low-temperature nitrogen adsorption (LTNA) experiment was performed on a Micromeritics ASAP 2460 surface area and porosity analyzer. The samples were processed into portions with weights of 2 g and grain sizes of 0.250.425 mm (4060 mesh). The particle samples were first dried in an oven at 60 °C (140 °F) for 24 h and degassed under a high vacuum (<10 mmHg) for 12 h at 110 °C (230 °F) in the apparatus to remove volatile substances and free water. According to the Kelvin equation, as the gas partial pressure of liquid increases, it condenses first in the smallest pores and then in larger pores. Based on this theory, Nitrogen adsorption-

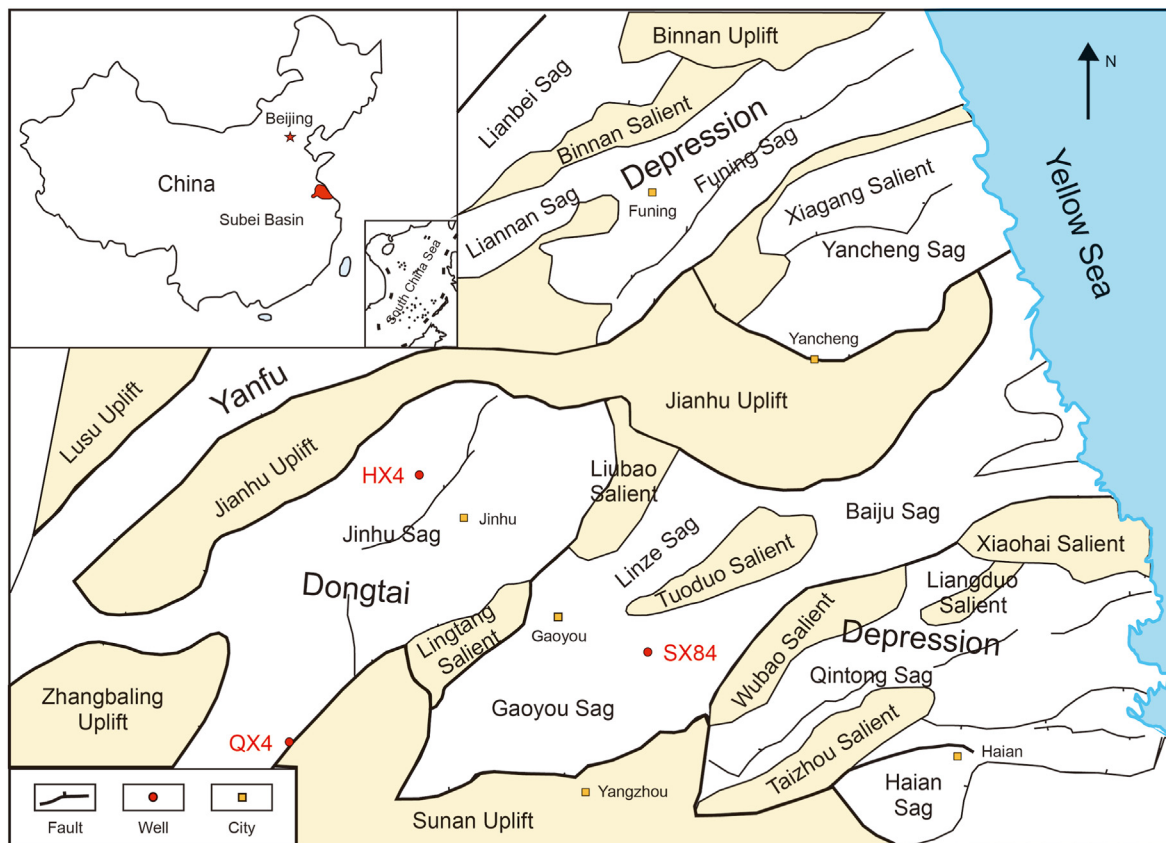


Fig. 1. Location and tectonic units of the Subei Basin (Song et al., 2010).

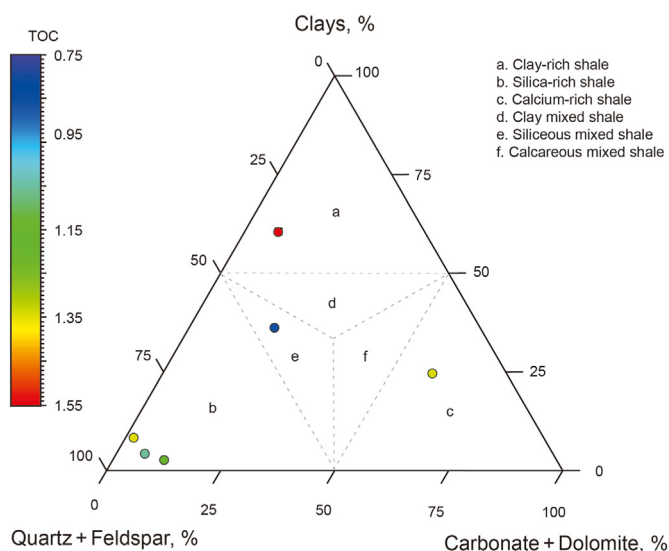


Fig. 2. Three terminal element diagram for lithology division of shale in the E₁f₂.

desorption isotherms were obtained under relative pressures (p/p_0) ranging from 0.01 to 0.993 at 77 K; The LTNA isotherms can provide information on the total pore volume, specific surface area, and PSD. In this study, the BET surface area was calculated from the LTNA data under relative pressure ranging from 0.05 to 0.35 using the multilayer adsorption theory proposed by Brunauer-Emmett-Teller (Brunauer et al., 1938). The total pore volume was estimated to be the liquid volume of the nitrogen adsorbed at a relative

pressure of 0.99. The PSD was used to identify the range of the dominant pore sizes and was obtained from the LTNA data using the Barrett-Joyner-Halenda (BJH) model (Barrett et al., 1951). According to the theoretical assumption of the model, the BJH model can well reflect the PSD of mesopores (2–50 nm), and the Kelvin equation can give the critical curvature radius of the pores. Therefore, the BJH model was used to calculate the PSD of the samples in this study.

3.2.3. Gas chromatography on saturated fractions

The Gas Chromatography (GC) experiments of shale oil in the study area were performed on an Agilent GC-MS 7890B-5977A (Agilent, USA). A nonpolar Rxi-5 phase column (60 m × 0.25 mm I.D. and 0.25 μm film thickness) was used. A small amount of extract was injected into a heated (300 °C) injector; GC temperature operating conditions for the saturated fraction were as follows: The oven temperature was initially set at 80 °C (5 min) and then to 300 °C (held 20 min) at 5 °C/min.

3.2.4. Rock-eval and multi-isothermal stage pyrolysis

Both standard Rock-eval (RE) pyrolysis and Multi-isothermal stages (MIS) pyrolysis were performed on the Rock-Eval VI apparatus with a flame ionization detector (FID).

For RE pyrolysis, the shale samples were crushed to a particle size of less than 0.150 mm, about 100 mg of sample was added to the pyrolysis oven to be heated to a programmed temperature, and the hydrocarbon gas volatilized and cracked under high temperature was separated from the sample residue by purging with inert gas (e.g., helium). The process of standard RE sequentially removes from the rock sample the gas, liquid, and solid components (S_0 , S_1 , and S_2 , respectively) of the oil by stepwise heating: the gaseous

hydrocarbon (S_0) in the rock is detected at the stage of 0–90 °C; then heated to 300 °C for 3 min to detect the liquid hydrocarbon (S_1), and then the temperature was raised to 600 °C at a rate of 25 °C/min to detect the gas generated by kerogen cracking and volatilization (S_2) (Espitalié et al., 1977; Lafargue et al., 1998; Behar et al., 2001).

In contrast, the process of MIS pyrolysis can be divided into four stages. S_{1-1} , representing the light molecular weight fraction, was obtained by heating from the ambient temperature at a rate of 25 °C/min to 200 °C for 1 min. Afterward, the sample was heated to 350 °C at a rate of 25 °C/min for 1 min to obtain S_{1-2} , composed of light and medium molecular weight fractions. Then the temperature was raised at the rate of 25 °C/min to 450 °C for 1 min to obtain S_{2-1} , composed of heavy hydrocarbons and polar compounds. Finally, the temperature was raised to 600 °C for 1 min to get S_{2-2} , representing kerogen cracking products.

3.2.5. Sequential solvent extraction

Sequential solvent extraction is widely used in the study of oil-bearing reservoirs. In this study, the free oil in the shale samples was obtained by cold ultrasonic extraction with dichloromethane, and the adsorbed oil was obtained by thermal extraction with tetrahydrofuran. Meanwhile, the samples and extracts after each extraction were collected and analyzed by various methods including LTNA, Rock pyrolysis, saturated hydrocarbon GC, and others (Fig. 3). The specific steps are as follows :

In the first step, the samples were surface-cleaned and cut into 6 or 7 cubes with a side length of about 1 cm. Then, the cubes were placed in a transparent airtight container containing an appropriate amount of dichloromethane. They were sonicated for 30 min in an ultrasonic cleaner with a frequency of 6 kHz, repeating the process until the color of the solvent did not change. The experiment was maintained at a constant temperature of 20 °C. After the extraction, the extracts were separated and analyzed by saturated hydrocarbon gas chromatography.

In the second step, the cubes that had been extracted in the first step were crushed into particles and sieved. The particle size fraction 0.85–2 mm was also subjected to the same experimental

procedure as in the first step. At the same time, the size fractions <0.150 mm and 0.25–0.425 mm that were obtained during the sample crushing process were subjected to RE pyrolysis and LTNA experiments, respectively. The extracts were also analyzed by gas chromatography.

In the third step, the extracted particle samples in the second step were further crushed to 0.25–0.425 mm. The extraction work of this step is completed on a rapid solvent extraction instrument (Beijing, Labtech). The extraction solvent adopts a more robust polar tetrahydrofuran reagent, and the extraction temperature is 100 °C. The extracts and shale samples were also subjected to GC, RE pyrolysis, and LTNA experiments.

4. Results

4.1. Types of shale reservoir space

The pore-fractures network is the main place and channel for shale oil storage and seepage. Generally, shale reservoir space can be divided into organic matter pores, intragranular pores, intergranular pores, and micro-fractures. The shale reservoir space selected in this study is dominated by inorganic pores, including clay mineral intragranular pores, feldspar dissolution pores, and calcite and quartz intergranular pores, while organic pores are hardly found. Thus, the inorganic pores and microfractures contribute to the primary occurrence space of shale oil (Fig. 4). The pores of silicon-rich shale are dominated by dissolution pores, which are mainly formed by feldspar dissolution under the action of organic acid. The pores are mostly filled with mixed-layer illite/smectite and authigenic quartz, and the pore shape is irregular, which is the key factor for a favorable shale oil reservoir (Fig. 4a–c). Intragranular pores of clay minerals are found in large quantities in clay-rich shale, which exists in flocculent clay mineral aggregates, and the pore morphology is mostly long strips and parallel plates (Fig. 4d). The pore space of calcium-rich shale and siliceous mixed shale is dominated by intergranular pores, which are formed between brittle mineral particles, and the pore morphology is relatively regular (Fig. 4e–f)

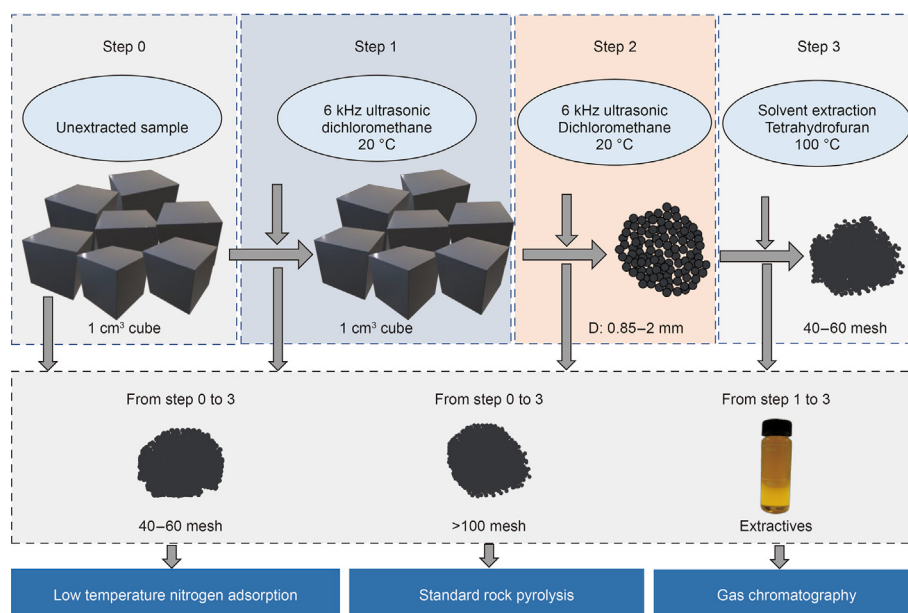


Fig. 3. Technical road.

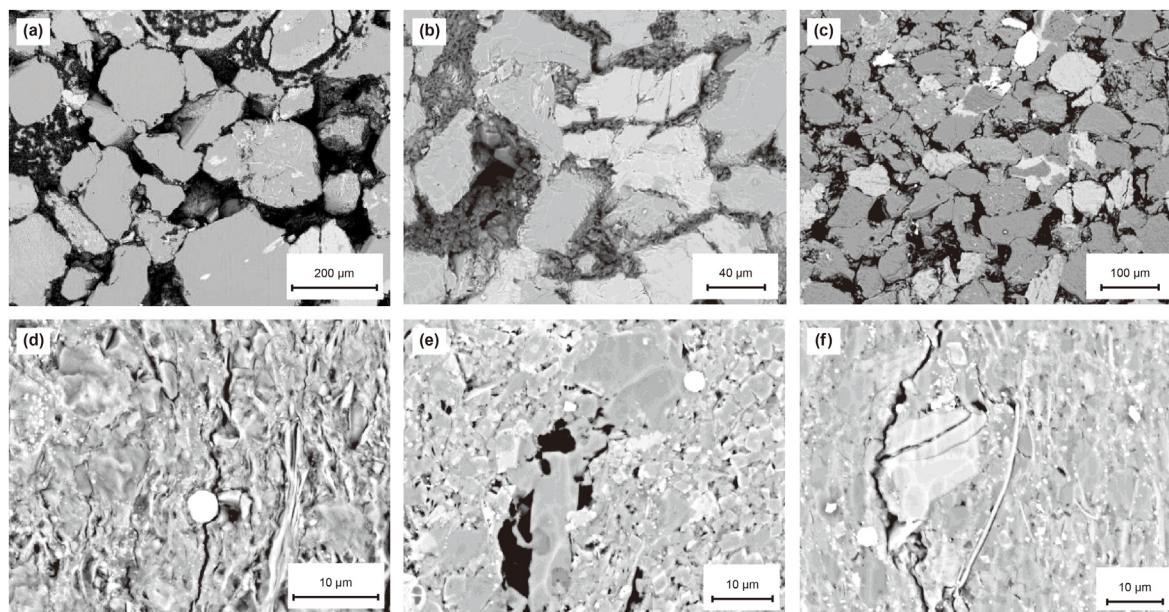


Fig. 4. Pore types of six shales. (a)–(f) represent HX4-3, QX4-1, QX4-2, SX84-20, SX84-8, and SX84-27, respectively.

4.2. Organic geochemical characteristics and composition

Standard RE pyrolysis and MIS pyrolysis data, performed through the standard procedure on the samples, are listed in Table 1. The organic matter maturity varies from low to mature with the pyrolysis hydrocarbon peak temperature (T_{max}) of 380–436 °C. S_1 represents the extractable free hydrocarbon content in the rock, which can directly reflect the degree of oil and gas enrichment of the rock, and the ranges from 0.97 to 5.99 mg/g, with an average value of 3.26 mg/g; The variation range of the hydrocarbon quantity parameter (S_2) of kerogen pyrolysis at high temperature is 1.78–9.58 mg/g (mean 5.07 mg/g). MIS pyrolysis parameters (i.e., S_{1-1} , S_{1-2} , S_{2-1} , and S_{2-2}) vary in a range of 0.07–0.22, 1.66–6.29, 1.41–4.95 and 0.16–2.06 mg/g, respectively. Among them, the pyrolysis yield, total oil, and free oil of silicon-rich shale (HX4-3, QX4-1, and QX4-2) are much higher than those of other lithologic shales (Table 1), which shows a good oil-bearing property for the silicon-rich shale.

The TOC of six samples varies from 0.86% to 1.52% (mean 1.21%) (Table 2). The inorganic material composition data obtained from XRD are listed in Table 2; the silicon-rich shales HX4-3, QX4-1, and QX4-2 are mainly composed of quartz and feldspar, which vary from 48.8% to 58.8% and 30.9%–38.51%, respectively with a small amount of calcite (1.57%–10.54%) and clay minerals (2.88%–4.2%). These are mainly in the form of sandstone interlayers in shale. The minerals of SX84-20 are dominated by dolomite (54.26%) and clay minerals (24.01%). The SX84-8 sample is mainly composed of clay

minerals (59.51%) and quartz (26.75%); while clays (29.21%), quartz (29%), and analcite (16.09%) are the dominant minerals of SX84-27.

4.3. Standard RE pyrolysis of extracted samples

The standard RE pyrolysis data of the extracted samples are shown in Table 3. Step 0 represents the original sample without extraction. The standard RE pyrolysis parameters (S_1 , S_2) of the six shale samples vary between 0.97 and 5.99 mg/g and 1.78–9.47 mg/g, respectively. The data of Step 1 are obtained from cubic samples with an edge length of about 1 cm in the cold ultrasonic extraction of methylene chloride; the pyrolysates of S_1 and S_2 are from 0.22 to 1.19 mg/g and 1.33–3.15 mg/g, respectively. The data in Step 2 refers to the standard RE pyrolysis after the cubes in Step 1 were crushed and sieved to 0.85–2 mm and then subjected to cold ultrasonic extraction. The S_1 and S_2 vary from 0.02 to 0.85 mg/g, and 0.83–2.24 mg/g, respectively. The data in Step 3 refers to the shale samples after two cold extractions that were further crushed and sieved to 0.25–0.425 mm and subjected to standard RE pyrolysis after thermal extraction. The pyrolysates of S_1 and S_2 vary in the range of 0.02–0.19 mg/g and 0.2–0.81 mg/g.

It can be clearly found that the pyrolysis yield decreases with the increase of extraction times, and the variation between pyrolysis steps can be represented by the parameters $\Delta(S_1+S_2)$, ΔS_1 , and ΔS_2 , i.e. the difference between two adjacent standards RE pyrolysis parameters, as shown in Fig. 5a–c, respectively. The original sample's RE pyrolysis yield (S_1+S_2) is the highest and gradually

Table 1

Peak pyrolysis temperature (T_{max}), Rock-Eval (RE) pyrolysis, and multiple isothermal stages (MIS) pyrolysis of shale samples.

Sample No.	T_{max} °C	Rock-Eval Pyrolysis		Multi-isothermal stages pyrolysis			
		S_1 , mg/g	S_2 , mg/g	S_{1-1} , mg/g	S_{1-2} , mg/g	S_{2-1} , mg/g	S_{2-2} , mg/g
HX4-3	429	5.99	7.47	0.22	6.29	4.10	0.93
QX4-1	428	5.32	9.58	0.11	6.19	4.95	1.73
QX4-2	436	3.54	6.64	0.07	4.60	3.63	2.06
SX84-20	408	2.67	3.13	0.14	3.17	2.37	0.62
SX84-8	380	1.07	1.80	0.09	2.12	1.43	0.16
SX84-27	383	0.97	1.78	0.08	1.66	1.41	0.27

Table 2
Total organic carbon (TOC) and inorganic minerals composition.

Sample No.	TOC %	Quartz %	Feldspar %	Calcite %	Dolomite %	Clays %	Pyrite %	Analcite %
HX4-3	1.15	48.08	38.51	10.54	0.00	2.88	0.00	0.00
QX4-1	1.33	55.08	35.07	1.57	0.00	8.28	0.00	0.00
QX4-2	1.06	58.80	30.90	4.00	2.10	4.20	0.00	0.00
SX84-20	1.32	13.33	2.58	3.31	54.26	24.01	1.09	1.42
SX84-8	1.52	26.75	4.74	2.88	4.19	59.51	1.92	0.00
SX84-27	0.86	29.00	8.45	2.67	12.69	29.91	1.19	16.09

Table 3
Standard RE pyrolysis data from extracted samples.

Sample No.	Step 0		Step 1		Step 2		Step 3	
	S ₁ , mg/g	S ₂ , mg/g	S ₁ , mg/g	S ₂ , mg/g	S ₁ , mg/g	S ₂ , mg/g	S ₁ , mg/g	S ₂ , mg/g
HX4-3	5.99	7.47	0.47	3.15	0.14	2.24	0.02	0.32
QX4-1	5.41	9.47	0.24	2.69	0.04	1.71	0.02	0.20
QX4-2	3.54	6.64	0.22	2.15	0.03	1.34	0.02	0.28
SX84-20	1.95	3.41	1.19	2.70	0.52	1.31	0.09	0.52
SX84-8	1.07	1.80	0.58	1.33	0.51	0.83	0.19	0.81
SX84-27	0.97	1.78	0.91	1.53	0.85	1.39	0.17	0.62

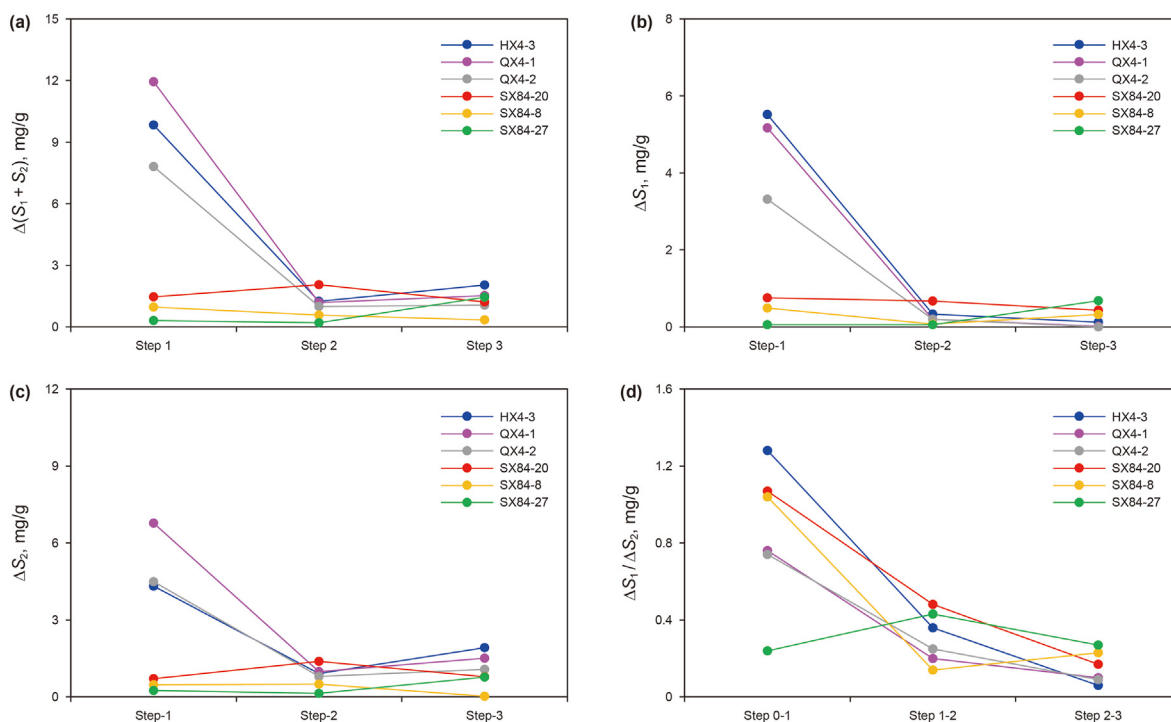


Fig. 5. Variation of shale standard RE pyrolysis parameters with the extraction process.

decreases with increased extraction times. $\Delta(S_1 + S_2)$ represents the total hydrocarbon reduction during standard RE pyrolysis, which varies from 0.31 to 11.95 mg/g (mean 5.39 mg/g), 0.2–2.06 mg/g (mean 1.04 mg/g), and 0.34–7.64 mg/g (mean 1.27 mg/g) after a single extraction, respectively (Fig. 5a). The content of ΔS_1 extracted at each step is 0.06–5.52 mg/g (mean 2.55 mg/g), 0.06–0.67 mg/g (mean 0.25 mg/g), and 0.002–0.68 mg/g (mean 0.26 mg/g), respectively (Fig. 5b). The ΔS_1 of Step 1 is much larger than that of Steps 2 and 3, which also verifies the experimental hypothesis, that is, the extracts of the first and second steps are mainly free oil with the light and medium soluble organic matter. Fig. 5c shows that the ΔS_2 varies in the range of 0.25–6.78 mg/g (mean 2.84 mg/g),

0.14–1.39 mg/g (mean 0.79 mg/g), and 0.02–1.92 mg/g (mean 1.01 mg/g) for steps 1, 2, and 3, respectively, which shows a trend of first decreasing and then increasing. The $\Delta S_1 / \Delta S_2$ values characterize the variation of free oil/adsorbed oil in shale reservoirs, which always show a decreasing trend during the step-by-step pyrolysis process (Fig. 5d).

4.4. The variation of soluble organic matter during sequential solvent extraction

The $(\Sigma n-C_{21} / \Sigma n-C_{22})$ ratio (sums of n-alkanes before C_{21} and after C_{22} , respectively) is used to characterize the distribution of n-

alkanes and to reveal further low and high molecular weight (LMW/HMW) ratio indicator (He et al., 2022a; 2022b). The peak areas of the n-alkanes were integrated to obtain a graph of the relative content of saturated hydrocarbons in a single extraction, as shown in Fig. 6d, where the relative content of each hydrocarbon (C_1 through C_{37}) is the ratio of the peak area of that hydrocarbon to the sum of the peak areas for all hydrocarbons (e.g., the relative content of C_{15} – C_{15} peak area/ $\sum C_i$ peak area, $i = 1, 2, \dots, 37$). The GC results of saturated hydrocarbons in sequential extracts are shown in Fig. 6. The dominant n-alkane peaks of shale extracts range from nC_{13} to nC_{38+} . And it gradually shifted from light-end bias to heavy-end bias with the increase in extraction times, indicating the variation of LMW/HMW proportion from Step 1 to Step 3, i.e., the dominant peak of n-alkanes shifted from C_{21} to C_{31} (Fig. 6a–c).

4.5. Characterization of occurrence space of shale oil with different states

The nitrogen adsorption isotherm curve of shale samples in Step 0–3 is shown in Fig. 7. It can be seen that although the isotherms of

shale samples are slightly different in shape, and they are all in the reverse "S" shape, that is, the type IV adsorption curve in the IUPAC classification. Moreover, at high relative pressures ($p/p_0 > 0.45$), the isotherms of the adsorption branch and the desorption branch do not coincide, and the desorption isotherm is located above the adsorption isotherm to form a hysteresis loop. The shape of the hysteresis loop can reflect the pore structure in the adsorbent. There are mainly two types of pore morphology in the shale samples studied in this study. The adsorption and desorption isotherms of Type I are almost parallel, and the hysteresis loop is long and narrow. The adsorption branch rises slowly when $p/p_0 < 0.9$ and rises rapidly after $p/p_0 > 0.9$, which is dominated by typical plate-like pores. Type II has a wide hysteresis loop, The variation of the desorption branch is relatively gentle when the relative pressure is high, and it becomes steeper at the medium relative pressure. Interestingly, after continuous solvent extraction of shale samples, the shape of low-temperature nitrogen adsorption isotherm has not changed, but the pore volume has slightly increased, indicating that shale oil may be desorbed from the surface of shale minerals in layers (Fig. 7).

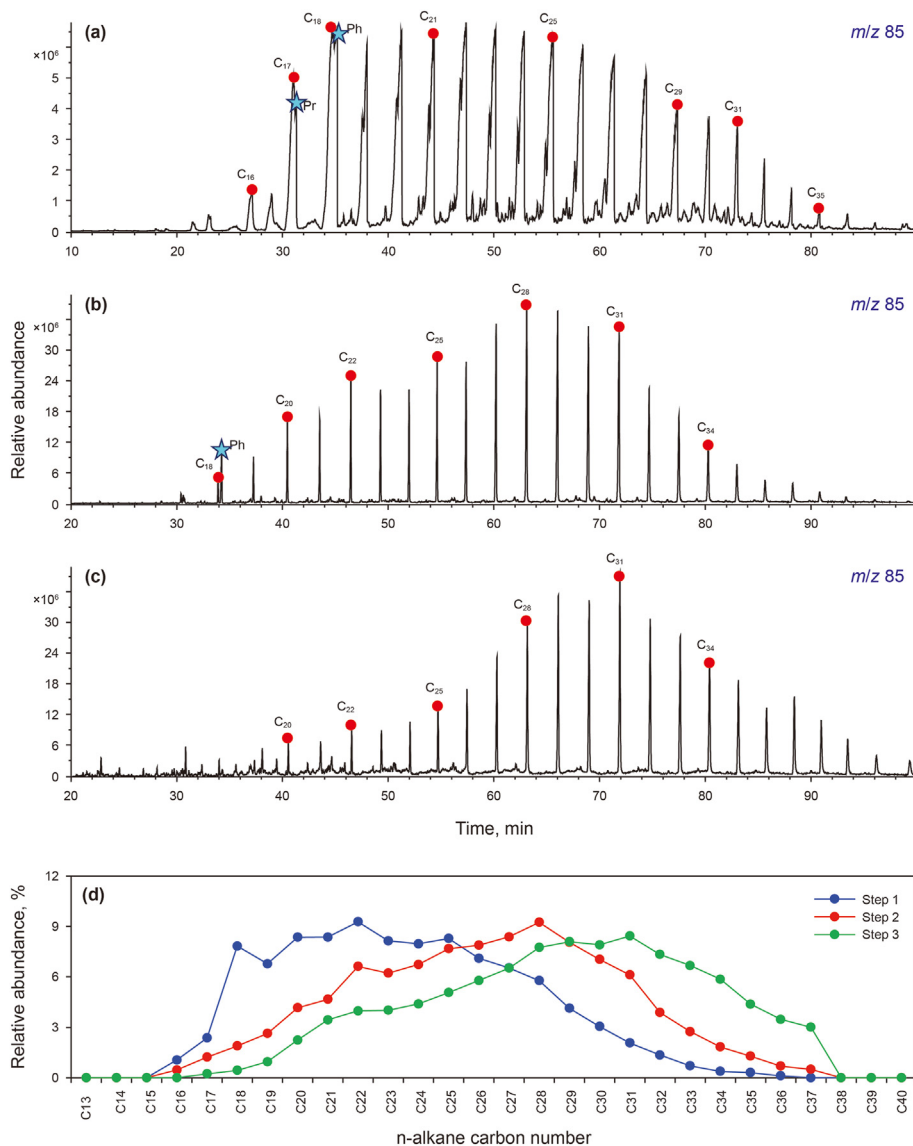


Fig. 6. Gas chromatogram of saturated hydrocarbon component m/z 85.

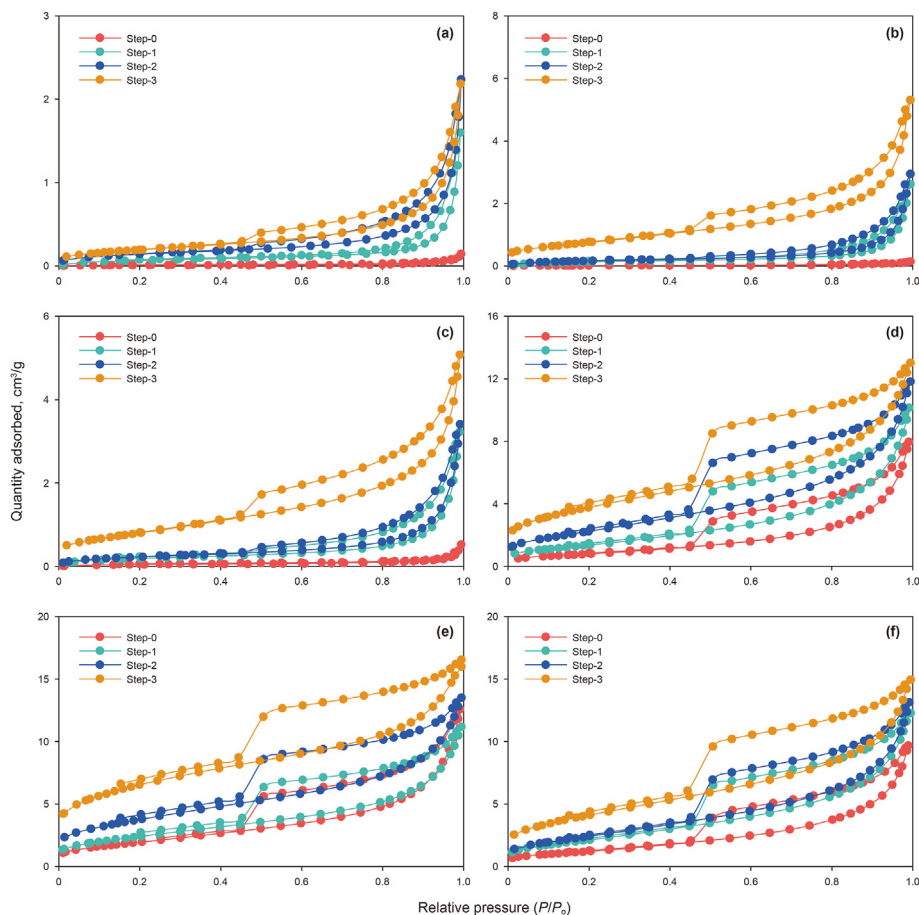


Fig. 7. Isotherm adsorption curves of steps 0 to 3. (a)–(f) represent HX4-3, QX4-1, QX4-2, SX84-20, SX84-8, and SX84-27, respectively.

The PSDs of shales after SSE are shown in Fig. 8. The analysis combined with GC data shows that the yellow area in Fig. 8 represents free oil dominated by medium and light hydrocarbons, while the orange area represents adsorbed oil dominated by heavy hydrocarbons. The occurrence characteristics of shale oil with different states in silicon-rich shale are different from other lithologic shales. The blue curve represents the PSD of the shales that have not been extracted. It can be seen that the absolute pore volume of the silicon-rich shale is significantly lower than that of the shale of other lithology. This is mainly because the pore space of the silicon-rich shale is occupied by retained hydrocarbons. After the first and second extraction, the pore space with PSD >10 nm in the silicon-rich shale is released, which indicates that the free oil in the silicon-rich shale mainly occurs in the pores with PSD above 10 nm. After the third extraction, the most significant change in absolute pore volume is the pore with PSD <20 nm, which indicates that the adsorbed oil in silicon-rich shale is mainly distributed in the pores with PSD <20 nm and it is also distributed in the pores with pore diameter >20 nm, but its proportion is relatively low.

In addition, the PSD of clay-rich shale, calcium-rich shale, and siliceous mixed shale is similar at Step 0, and the samples have relatively large pore volumes. After the first and second extraction, the space occupied by free oil is released. Compared with clay-rich shale, calcium-rich shale, and siliceous mixed shale show relatively more significant pore volume increment, which is mainly contributed by pores with PSD of 2–30 nm, indicating that free oil in calcium-rich shale and siliceous mixed shale is mainly distributed in pores with PSD of 2–30 nm, while free oil in clay-rich shale is

mainly distributed in pores with PSD of <10 nm. The extraction results in the third step show that the adsorbed oil in calcium-rich shale, clay-rich shale, and siliceous mixed shale mainly occurs in the PSD <10 nm or even smaller.

5. Discussion

5.1. Comparison of the total hydrocarbon between sequential solvent extraction, RE, and MIS pyrolysis

MIS pyrolysis and RE pyrolysis are effective methods to evaluate source rocks' hydrocarbon generation potential and in-situ hydrocarbon content. However, standard RE pyrolysis suffers from delayed detection of heavy hydrocarbons and non-hydrocarbons and incorrect estimation of asphaltenes. MIS pyrolysis further subdivides the rock pyrolysis process based on standard RE pyrolysis, which is an advanced method for evaluating the content of shale oil at present. Although there are some errors in standard RE pyrolysis, they should be consistent in evaluation parameters (e.g., hydrocarbon generation potential). In this study, Correlations between standard RE pyrolysis parameters (S_1 , S_2) and MIS pyrolysis parameters (S_{1-1} , S_{1-2} , S_{2-1} , S_{2-2}) of the non-extracted samples (Step 0) were analyzed (Fig. 9; lines are forced through the origin). The results show that the two pyrolysis methods have good consistency in the evaluation of hydrocarbon generation potential (S_1+S_2 & $S_{1-1}+S_{1-2}+S_{2-1}+S_{2-2}$) (Fig. 9a), and the total oil ($S_1+S_2-S_{2-2}$ & $S_{1-1}+S_{1-2}+S_{2-1}$), free oil (S_1 & $S_{1-1}+S_{1-2}$) and adsorbed oil (S_2-S_{2-2} & S_{2-1}) obtained by RE pyrolysis are about 90%, 83% and 144% of those

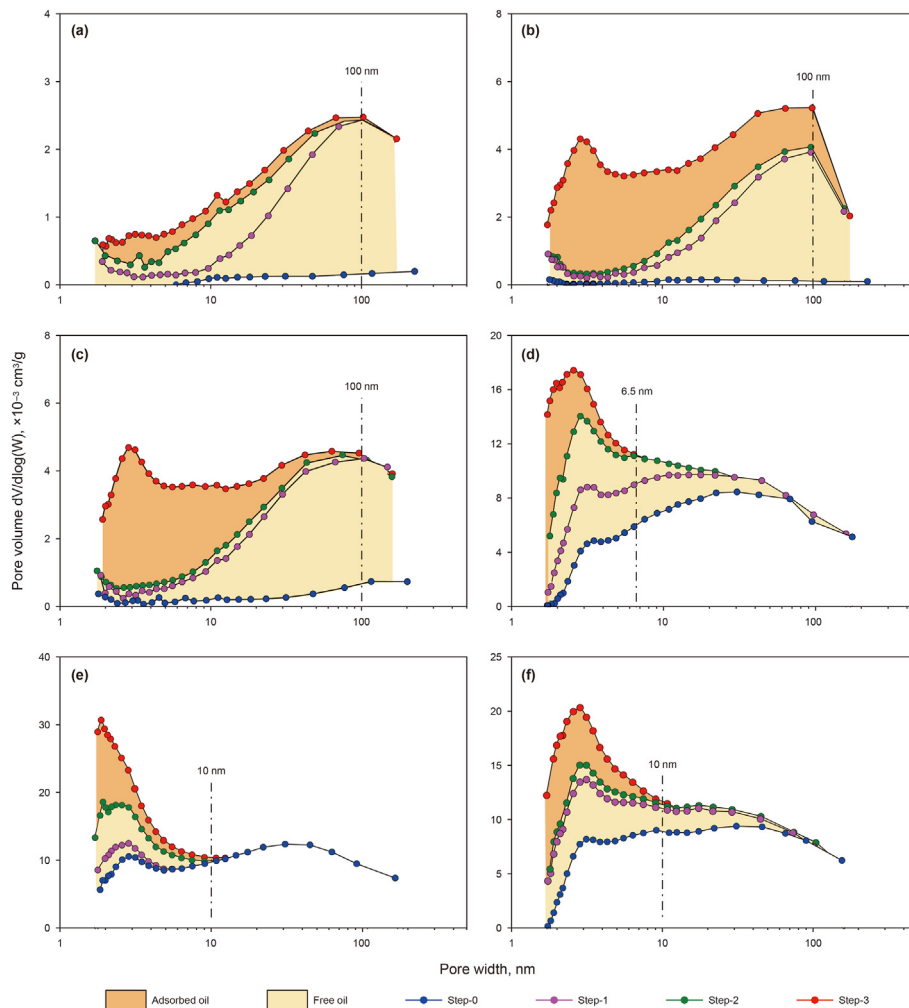


Fig. 8. PSD of the BJH model for each step of the sequential solvent extraction process. (a)–(f) represent HX4-3, QX4-1, QX4-2, SX84-20, SX84-8, and SX84-27, respectively.

obtained by MIS pyrolysis, respectively (Fig. 9b, c, and d). Therefore, the standard RE pyrolysis can still be used as an effective method to evaluate the contents of shale oil in different states.

The sequential solvent extraction (SSE) method can reflect crude oil's multi-layer structure and distinguish free and adsorbed oil in shale reservoirs (Pan and Liu, 2009; Yu et al., 2017). In this study, based on the SSE experiment, the standard RE pyrolysis test was carried out for shale after each extraction. The difference between two adjacent standard RE pyrolysis parameters ($\Delta S_1 + \Delta S_2$) was used to reflect the variation of extracted content in shale. The cumulative variation of the extract after three times extractions was compared with the MIS pyrolysis data of the non-extracted samples to reflect the consistency between the total amount of the extract and the total amount of pyrolysis. It was found that the amount of shale oil extracted by the SSE method is about 1.17 times that of the MIS pyrolysis method ($S_{1-1} + S_{1-2} + S_{2-1}$) (Fig. 10a). After correcting the total oil amount of standard RE pyrolysis and MIS pyrolysis, the actual amount of shale oil calculated by SSE method is about 1.089 times that of MIS pyrolysis, which indicates that the SSE method is accurate and reliable for evaluating the content of shale oil in the matrix. However, the quantitative characterization of the content of free oil and adsorbed oil by SSE is slightly different from that of MIS pyrolysis. The content of adsorbed oil and free oil in SSE is 1.68 times and 0.8 times of MIS pyrolysis data, respectively (Fig. 10b and c). Therefore, the ratio of free oil to adsorbed oil evaluated by the

SSE method is about half of that of MIS pyrolysis (Fig. 5d).

5.2. Comparison between pore volume increment and hydrocarbon generation potential

The relationship between pore volume, a key parameter for evaluating reservoir performance, and the variation of the pyrolysis yield is discussed. Soluble organic matter in shale usually occupies a specific pore volume, gradually releasing as the soluble organic matter is dissolved. Fig. 11 shows that the variation trend of the hydrocarbon generation potential ($\Delta S_1 + \Delta S_2$) is in good agreement with the pore volume ($\Delta \text{Pore volume}$), which indicates that the extraction of residual oil in the pores is the main reason for the increase of pore volume, although the two cannot perfectly coincide, which is mainly due to the destruction of larger pores and fractures in the process of rock fragmentation. Damage to rock pore structure caused by the organic solvent used in extraction process and the limitation of PSD for LTNA techniques.

5.3. Analysis of the shale oil occurrence characteristics beyond the limit of LTNA

LTNA method can effectively reflect the distribution of nanopores in materials, and the PSD for shale testing is between 2 and 300 nm, which has been widely used in shale micropore structure

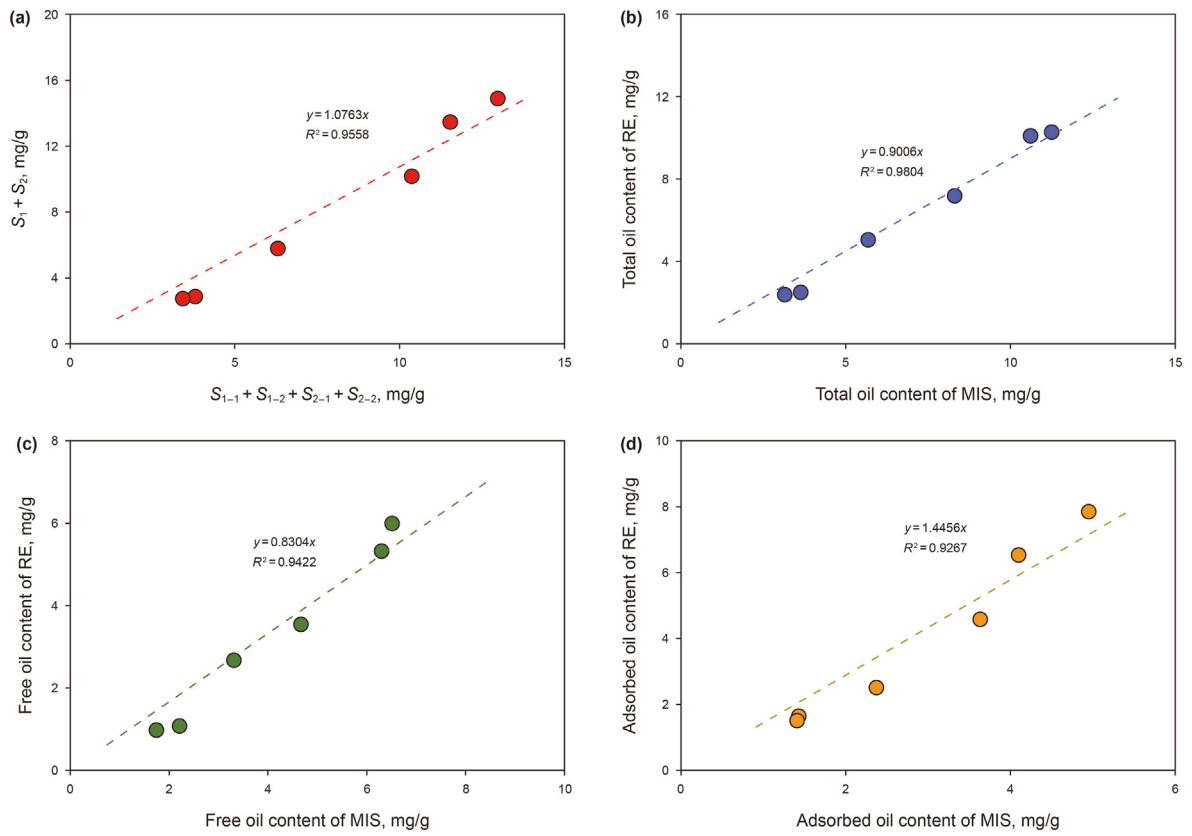


Fig. 9. Comparison of critical parameters between standard RE pyrolysis and MIS pyrolysis.

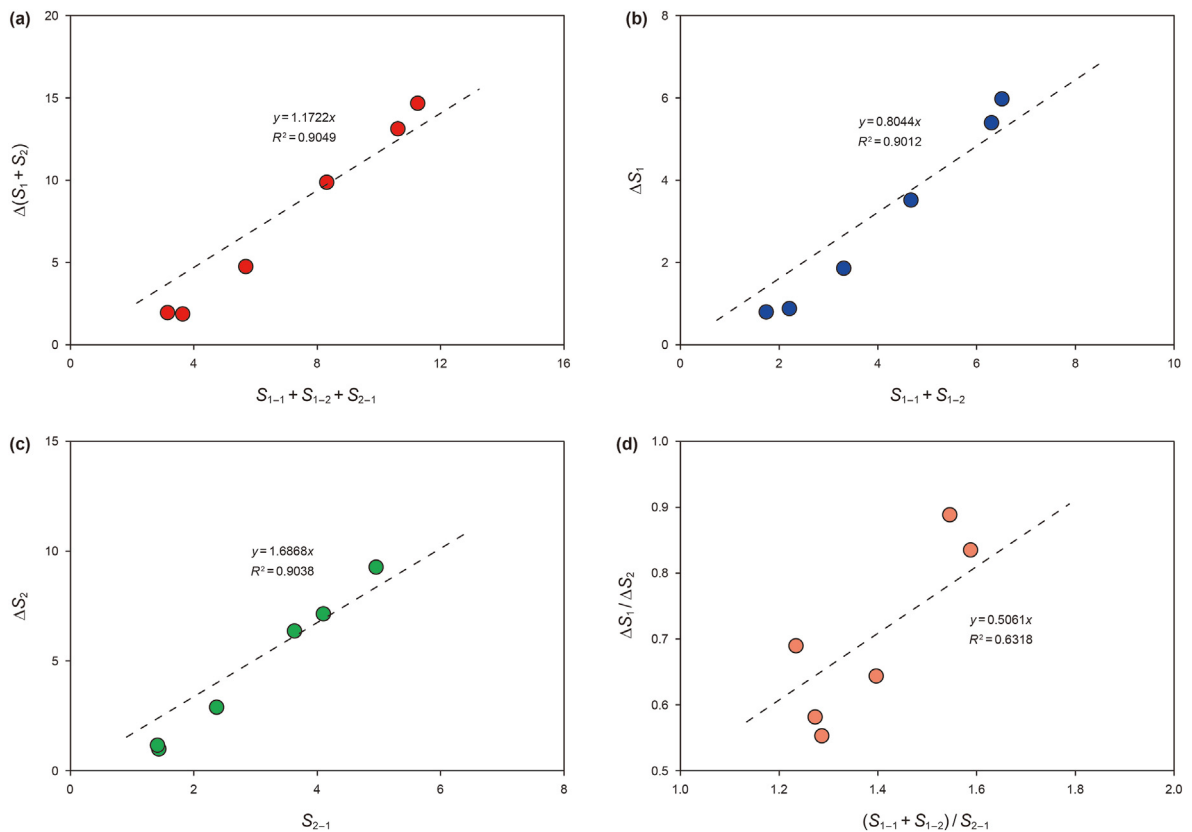


Fig. 10. Comparison of total oil content, adsorbed oil, and free oil content between SSE and MIS pyrolysis.

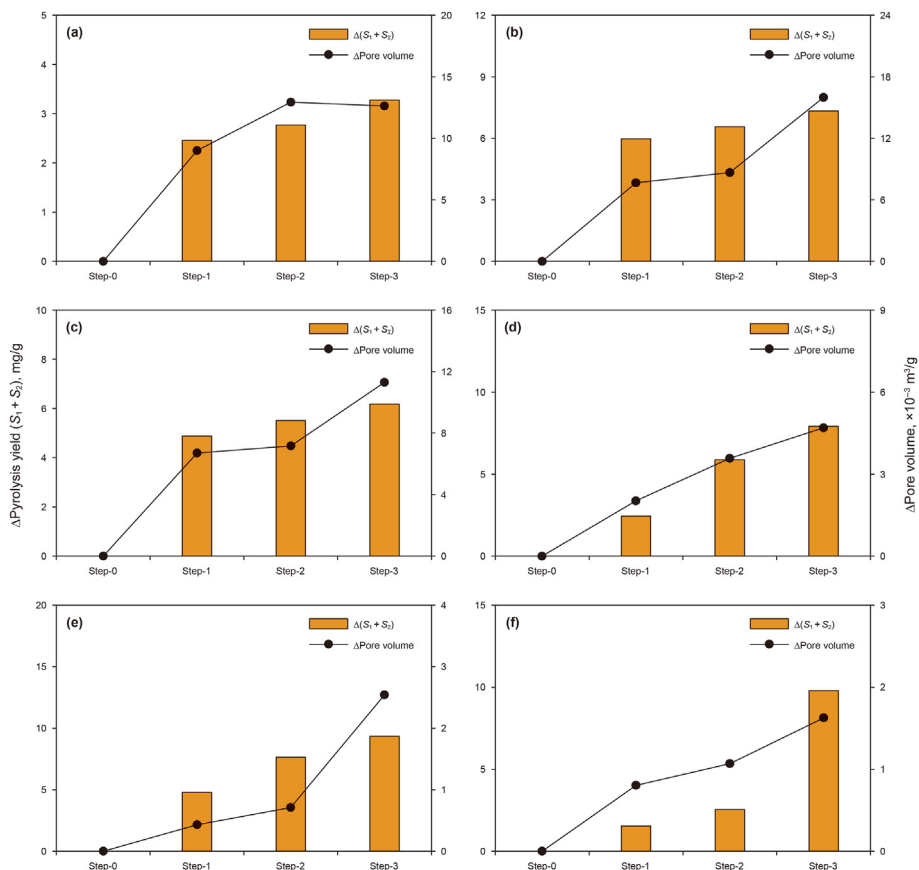


Fig. 11. Correlation of Δ Pyrolysis yield (S_1+S_2) with Δ Pore volume.

testing. Although this scale can detect most nanopores, it is still a little insufficient for the fractures existing in the shale matrix, which challenges us to characterize the occurrence characteristics of oil in the shale matrix on a full scale. However, the occurrence states and proportion of shale oil in pores with PSD larger than 200 nm can still be inferred according to the variation of shale oil in different occurrence states at the PSD of 2–200 nm. Fig. 12 shows the variation of the relative content of shale oil with PSD in different occurrence states. Among them, the relative content of free oil in silicon-rich shale decreases in the pore size of 2–3 nm and gradually reaches 100% in the pore size of 3–200 nm. The relative content of free oil in calcium-rich shale, clay-rich shale, and

siliceous mixed shale only increases with the pore size and reaches 100% at 10 nm, but the PSD of adsorbed oil is just opposite to that of free oil. Therefore, the distribution trend of shale oil in different states in the more extensive PSD can be inferred, that is, in the silicon-rich shale, the relative content of free oil is dominant in the pores with PSD larger than 200 nm or in the PSD greater than 10 nm in the calcium-rich shale, clay-rich shale, and siliceous mixed shale, while the proportion of adsorbed oil is very small.

6. Conclusions

In this study, organic geochemistry and pore structure

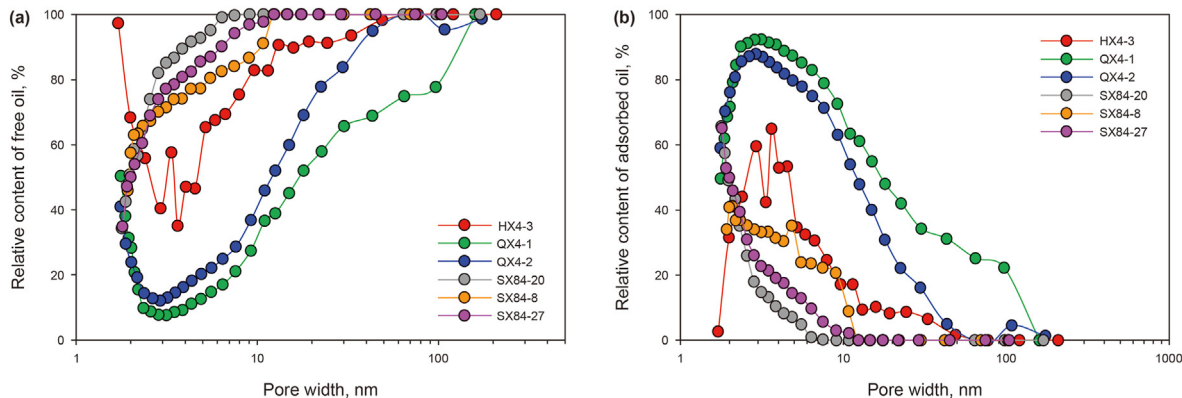


Fig. 12. Variation of the relative content of shale oil with PSD in different occurrence states.

characterization technology were combined to characterize the occurrence characteristics of shale oil quantitatively. The data of MIS pyrolysis show that the content of total oil, adsorbed oil, and free oil are 3.15–11.25 mg/g, 1.41–4.95 mg/g, and 1.74–6.51 mg/g, respectively, which is consistent with that obtained by SSE method.

The difference in the PSD of free oil and adsorbed oil in different lithologic shale is noticeable. The relative content of free oil in silicon-rich shale decreases first and then increases at the turning point of 3 nm and reaches 100% when the pore size is about 200 nm. The relative content of free oil in calcium-rich shale, clay-rich shale, and siliceous mixed shale increases with the increase of pore size and reaches 100% when the pore size is about 10 nm, while the PSD of adsorbed oil in shale is opposite to that of free oil, which indicates that shale oil will occur in the pores and fractures in a free state in a more extensive pore size range (>200 nm).

The combined organic geochemical and pore structure characterization technology is an effective means to study the occurrence characteristics of shale oil, and further research is needed to generalize this work, which could include: (1) Unexposed shale is needed to evaluate in situ shale oil occurrence characteristics, e.g., shale frozen with liquid nitrogen, shale of sealed coring, etc. (2) Whether this method applies to shale with different maturity.

Declaration of competing interest

The authors declare that they have no known competing financial interests or personal relationships that could have appeared to influence the work reported in this paper.

Acknowledgments

This work was financially supported by the National Natural Science Foundation of China (41972123, 41922015), and the Natural Science Foundation of Shandong Province (ZR2020QD036).

Acronyms

RE	standard rock-eval pyrolysis
MIS	multiple isothermal stages pyrolysis
SSE	sequential solvent extraction
ESEM	environmental scanning electron microscopy
B-AOWNA	nitrogen adsorption before and after oil washing
2D-NMR	two-dimensional nuclear magnetic resonance
LTNA	low-temperature nitrogen adsorption
SSA	specific surface area
RPV	relative pore volume
APV	absolute pore volume
PSD	pore size distribution
LMW	low molecular weight
HMW	high molecular weight
BJH	Barrett-Joyner-Halenda
BET	Brunauer-Emmett-Teller

References

Abrams, M.A., Gong, C.R., Gamier, C., Sephton, M.A., 2017. A new thermal extraction protocol to evaluate liquid rich unconventional oil in place and in-situ fluid chemistry. *Mar. Petrol. Geol.* 88, 659–675. <https://doi.org/10.1016/j.marpetgeo.2017.09.014>.

Barrett, E.P., Joyner, L.G., Halenda, P.P., 1951. The determination of pore volume and area distributions in porous substances. I. Computations from nitrogen isotherms. *J. Am. Chem. Soc.* 73, 30–319. <https://doi.org/10.1021/ja01145a126>.

Behar, F., Beaumont, V., Pentead, H.L., 2001. Rock-Eval 6 technology: performances and developments. *Oil Gas Sci. Technol.* 56, 111–134. <https://doi.org/10.2516/ogst:2001013>.

Brunauer, S., Emmett, P.H., Teller, E., 1938. Adsorption of gases in multimolecular layers. *J. Am. Chem. Soc.* 60, 309–319. <https://doi.org/10.1021/ja01269a023>.

Chen, X.H., 2017. Advances in the research on the occurrence state and resources

assessment of shale oil. *Sci. Technol. Eng.* 17, 136–144. <https://doi.org/10.3969/j.issn.1671-1815.2017.03.020>.

Dang, W., Nie, H.K., Zhang, J.C., Tang, X., Jiang, S., Wei, X.L., Liu, Y., Wang, F.Q., Li, P., Chen, Z.P., 2022. Pore-scale mechanisms and characterization of light oil storage in shale nanopores: new method and insights. *Geosci. Front.* 13, 101424. <https://doi.org/10.1016/j.gsf.2022.101424>.

Dong, C.Y., Liu, Z., Liu, Q.D., Luo, B.W., Li, C.H., Wang, W.J., 2013. Accumulation system and controlling factors reservoirs of Dainan Formation in Gaoyou sag of fault-lithologic northern Jiangsu Basin. *Petrol. Exp. Geol.* 35, 395–400. <https://doi.org/10.11781/sydz201304395>.

Espitalié, J., Laporte, J.L., Madec, M., Marquis, F., Leplat, P., Paulet, J., Boutefeu, A., 1977. Méthode rapide de caractérisation des roches mères, de leur potentiel pétrolier et de leur degré d'évolution. *Rev. Inst. Fr. Pet.* 32, 23–42. <https://doi.org/10.2516/ogst:1977002>.

Feng, Q.H., Xu, S.Q., Xing, X.D., Zhang, W., Wang, S., 2020. Advances and challenges in shale oil development: a critical review. *Adv. Geo-Energy Res.* 4, 406–418. <https://doi.org/10.46690/ager.2020.04.06>.

Gang, W.Z., Gao, G., Wang, Y., Shen, X., 2012. The original Types of Paleogene crude oils in Gaoyou Sag and their migration-accumulation models. *J. Shandong Univ. Sci. Technol. (Nat. Sci.)* 31, 21–28. <https://doi.org/10.3969/j.issn.1672-3767.2012.01.003>.

He, T.H., Li, W.H., Lu, S.F., Yang, E.Q., Jing, T.T., Ying, J.F., Zhu, P.F., Wang, X.Z., Pan, W.Q., Zhang, B.S., Chen, Z.H., 2022a. Quantitatively unmixing method for complex mixed oil based on its fractions carbon isotopes: a case from the Tarim Basin, NW China. *Petrol. Sci.* 2022, 20 (1), 102–113. <https://doi.org/10.1016/j.petsci.2022.07.010>.

He, T.H., Li, W.H., Lu, S.F., Yang, E.Q., Jing, T.T., Ying, J.F., Zhu, P.F., Wang, X.Z., Pan, W.Q., Chen, Z.H., 2022b. Distribution and isotopic signature of 2-alkyl-1,3,4-trimethylbenzenes in the Lower Paleozoic source rocks and oils of Tarim Basin: implications for the oil-source correlation. *Petrol. Sci.* 2022, 19 (6), 2572–2582. <https://doi.org/10.1016/j.petsci.2022.07.014>.

Hu, S.Y., Zhao, W.Z., Hou, L.H., Yang, Z., Zhu, R.K., Wu, S.T., Bai, B., Jin, X., 2020. Development potential and technical strategy of continental shale oil in China. *Petrol. Explor. Dev.* 47, 877–887. [https://doi.org/10.1016/S1876-3804\(20\)60103-3](https://doi.org/10.1016/S1876-3804(20)60103-3).

Hu, T., Pang, X.Q., Jiang, S., Wang, Q.F., Zheng, X.W., Ding, X.G., Zhao, Y., Zhu, C.X., Li, H., 2018. Oil content evaluation of lacustrine organic-rich shale with strong heterogeneity: a case study of the Middle Permian Lucaogou Formation in Jimusaer Sag, Junggar Basin, NW China. *Fuel* 221, 196–205. <https://doi.org/10.1016/j.fuel.2018.02.082>.

Hu, T., Pang, X.Q., Jiang, F.J., Wang, Q.F., Wu, G.Y., Liu, X.H., Jiang, S., Li, C.R., Xu, T.W., Chen, Y.Y., 2021a. Key factors controlling shale oil enrichment in saline lacustrine rift basin: implications from two shale oil wells in Dongpu Depression, Bohai Bay Basin. *Petrol. Sci.* 18, 687–711. <https://doi.org/10.1007/s12182-021-00564-z>.

Hu, T., Pang, X.Q., Jiang, F.J., Wang, Q.F., Liu, X.H., Wang, Z., Jiang, S., Wu, G.Y., Li, C.J., Xu, T.W., Li, M.W., Yu, J.W., Zhang, C.X., 2021b. Movable oil content evaluation of lacustrine organic-rich shales: methods and a novel quantitative evaluation model. *Earth Sci. Rev.* 214, 103545. <https://doi.org/10.1016/j.earscirev.2021.103545>.

Jarvie, D.M., 2012. Shale resource systems for oil and gas: Part 2—shale-oil resource systems. In: Breyer, J.A. (Ed.), *Shale Reservoirs—Giant Resources for the 21st Century*, vol. 97. AAPG Memoir, pp. 89–119. <https://doi.org/10.1306/13321447M973489>.

Jia, C.Z., Zou, C.N., Li, J.Z., Li, D.H., Zhang, M., 2012. Assessment criteria, main types, basic features and resource prospects of the tight oil in China. *Acta Petrol. Sin.* 33, 343–350. <https://doi.org/10.7623/syxb201203001>.

Jiang, C.J., Chen, Z.H., Mort, A., Milovic, M., Robinson, R., Stewart, R., Lavoie, D., 2016. Hydrocarbon evaporative loss from shale core samples as revealed by Rock-Eval and thermal desorption-gas chromatography analysis: its geochemical and geological implications. *Mar. Petrol. Geol.* 70, 294–303. <https://doi.org/10.1016/j.marpetgeo.2015.11.021>.

Jiang, Q.G., Li, M.W., Qian, M.H., Li, Z.M., Li, Z., Huang, Z.K., Zhang, C.M., Ma, Y.Y., 2016. Quantitative characterization of shale oil in different occurrence states and its application. *Petrol. Geol. Exp.* 38, 842–849. <https://doi.org/10.11781/sydz201606842>.

Lafargue, E., Marquis, F., Pillot, D., 1998. Rock-Eval 6 applications in hydrocarbon exploration, production, and soil contamination studies. *Rev. Inst. Fr. Pet.* 53, 421–437. <https://doi.org/10.2516/ogst:1998036>.

Li, J.Q., Lu, S.F., Cai, J.C., Zhang, P.F., Xue, H.T., Zhao, X.B., 2018. Adsorbed and free oil in lacustrine nanoporous shale: a theoretical model and a case study. *Energy Fuel.* 32, 12247–12258. <https://doi.org/10.1021/acs.energyfuels.8b02953>.

Li, J.Q., Lu, S.F., Xie, L.J., Zhang, J., Xue, H.T., Zhang, P.F., Tian, S.S., 2017. Modeling of hydrocarbon adsorption on continental oil shale: a case study on n-alkane. *Fuel* 206, 603–613. <https://doi.org/10.1016/j.fuel.2017.06.017>.

Lin, Z.Z., Li, J.Q., Wang, M., Zhang, P.F., Lu, S.F., Zhi, Q., Wang, J.J., Huang, H.S., 2022. Organic fluid migration in low permeability reservoirs restricted by pore structure parameters. *J. Petrol. Sci. Eng.*, 111028. <https://doi.org/10.1016/j.petrol.2022.111028>.

Liu, B., Bai, L.H., Chi, Y.A., Ru, J., Fu, X.F., Yang, L., 2019. Geochemical characterization and quantitative evaluation of shale oil reservoir by two-dimensional nuclear magnetic resonance and quantitative grain fluorescence on extract: a case study from the Qingshankou Formation in Southern Songliao Basin, northeast China. *Mar. Petrol. Geol.* 109, 561–573. <https://doi.org/10.1016/j.marpetgeo.2019.06.046>.

- Liu, S.L., Duan, H.L., Zhang, Y., Wang, H.W., Gao, J., 2014. Analysis of oil and gas exploration potential in F2 member continental shale of Subei Basin. *Offshore Oil* 34, 27–33. [10.1008-2336.2014.03.027](https://doi.org/10.1008-2336.2014.03.027).
- Lu, S.F., Xue, H.T., Wang, M., Xiao, D.S., Huang, W.B., Li, J.Q., Xie, L.J., Tian, S.S., Wang, S., Li, J.J., Wang, W.M., Chen, F.W., Li, W.H., Xue, Q.Z., Liu, X.F., 2016. Several key issues and research trends in evaluation of shale oil. *Acta Petrol. Sin.* 37, 1309–1322. <https://doi.org/10.7623/syxb201610012>.
- Ning, F.X., Wang, X.J., Hao, X.F., Yang, W.Q., Yin, Y., Ding, J.H., Zhu, D.Y., Zhu, D.S., Zhu, J.J., 2017. Occurrence mechanism of shale oil with different lithofacies in Jiyang Depression. *Acta Petrol. Sin.* 38, 185–195. <https://doi.org/10.7623/syxb201702006>.
- Pan, C.C., Liu, D.Y., 2009. Molecular correlation of free oil, adsorbed oil and inclusion oil of reservoir rocks in the Tazhong Uplift of the Tarim Basin. *China. Org. Geochem.* 40, 387–399. <https://doi.org/10.1016/j.orggeochem.2008.11.005>.
- Regtop, R.A., Crisp, P.T., Ellis, J., 1982. Chemical characterization of shale oil from Rundle, Queensland. *Fuel* 61, 185–192. [https://doi.org/10.1016/0016-2361\(82\)90233-2](https://doi.org/10.1016/0016-2361(82)90233-2).
- Romero-Sarmiento, M.F., Pillot, D., Letort, G., Lamoureux-Var, V., Beaumont, V., Huc, A.Y., Garcia, B., 2016. New Rock-Eval method for characterization of unconventional shale resource systems. *Oil. Gas Sci. Technol-Revue D'IFP Energies Nouvelles*. 71, 37–46. <https://doi.org/10.2516/ogst/2015007>.
- Sajgó, C., Maxwell, J.R., Mackenzie, A.S., 1983. Evaluation of fractionation effects during the early stages of primary migration. *Org. Geochem.* 5, 65–73. [https://doi.org/10.1016/0146-6380\(83\)90004-9](https://doi.org/10.1016/0146-6380(83)90004-9).
- Schwark, L., Stoddart, D., Keuser, C., Spitthoff, B., Leythaeuser, D., 1997. A novel sequential extraction system for whole core plug extraction in a solvent flow-through cell—application to extraction of residual petroleum from an intact pore-system in secondary migration studies. *Org. Geochem.* 26, 19–31. [https://doi.org/10.1016/S0146-6380\(96\)00163-5](https://doi.org/10.1016/S0146-6380(96)00163-5).
- Song, N., Wang, T.G., Chen, L.Q., Xin, R.C., 2010. Comprehensive analysis on hydrocarbon accumulation period of upper cretaceous Taizhou Formation in northern Jiangsu Basin. *Acta Pet. Sin.* 31, 180–187. <https://doi.org/10.7623/syxb201002002>.
- Wang, M., Ma, R., Li, J.B., Lu, S.F., Li, C.M., Guo, Z.Q., Li, Z., 2019. Occurrence mechanism of lacustrine shale oil in the paleogene shahejie formation of jiyang depression, bohai bay basin, China. *Petrol. Explor. Dev.* 46, 833–846. [https://doi.org/10.1016/S1876-3804\(19\)60242-9](https://doi.org/10.1016/S1876-3804(19)60242-9).
- Wang, W.Y., Pang, X.Q., Wang, Y.P., Chen, Z.X., Li, C.R., Ma, X.H., 2022. Hydrocarbon expulsion model and resource potential evaluation of high-maturity marine source rocks in deep basins: example from the Ediacaran microbial dolomite in the Sichuan Basin. *China. Petrol. Sci.* 19, 2618–2630. <https://doi.org/10.1016/j.petsci.2022.11.018>.
- Wilhelms, A., Horstad, I., Karlsen, D., 1996. Sequential extraction—a useful tool for reservoir geochemistry? *Org. Geochem.* 24, 1157–1172. [https://doi.org/10.1016/S0146-6380\(96\)00100-3](https://doi.org/10.1016/S0146-6380(96)00100-3).
- Xu, Y., Lun, Z.M., Pan, Z.J., Wang, H.T., Zhou, X., Zhao, C.P., Zhang, D.F., 2022. Occurrence space and state of shale oil: a review. *J. Petrol. Sci. Eng.*, 110183. <https://doi.org/10.1016/j.petrol.2022.110183>.
- Yu, S., Wang, X.L., Xiang, B.L., Ren, J.L., Li, E.T., Wang, J., Huang, P., Wang, G.B., Xu, H., Pan, C.C., 2017. Molecular and carbon isotopic geochemistry of crude oils and extracts from Permian source rocks in the northwestern and central Junggar Basin. *China. Org. Geochem.* 113, 27–42. <https://doi.org/10.1016/j.orggeochem.2017.07.013>.
- Zhang, H., Huang, H.P., Li, Z., Liu, M., 2020. Comparative study between sequential solvent-extraction and multiple isothermal stages pyrolysis: a case study on Eocene Shahejie Formation shales, Dongying Depression, East China. *Fuel* 263, 116591. <https://doi.org/10.1016/j.fuel.2019.116591>.
- Zhang, P.F., Lu, S.F., Li, J.Q., Chang, X.C., Lin, Z.Z., Chen, G., Li, J.J., Liu, J.Z., Tian, S.S., 2022a. Evaluating microdistribution of adsorbed and free oil in a lacustrine shale using nuclear magnetic resonance: a theoretical and experimental study. *J. Petrol. Sci. Eng.* 212, 110208. <https://doi.org/10.1016/j.petrol.2022.110208>.
- Zhang, P.F., Lu, S.F., Lin, Z.Z., Duan, H.L., Chang, X.C., Qiu, Y.F., Fu, Q., Zhi, Q., Wang, J.J., Huang, H.S., 2022b. Key oil content parameter correction of shale oil resources: a case study of the paleogene Funing Formation, Subei Basin, China. *Energy Fuel*. 36, 5316–5326. <https://doi.org/10.1021/acs.energyfuels.2c00610>.
- Zhu, C.F., Guo, W., Li, Y.J., Gong, H.J., Sheng, J.J., Dong, M.Z., 2021. Effect of occurrence states of fluid and pore structures on shale oil movability. *Fuel* 288, 119847. <https://doi.org/10.1016/j.fuel.2020.119847>.
- Zink, K.G., Scheeder, G., Stueck, H.L., Biermann, S., Blumenberg, M., 2016. Total shale oil inventory from an extended Rock-Eval approach on non-extracted and extracted source rocks from Germany. *Int. J. Coal Geol.* 163, 186–194. <https://doi.org/10.1016/j.coal.2016.06.023>.